Failure behaviour of metal inserts embedded in CFRP subsequent to thermal, mechanical and cyclic pre-damage

Markus Muth, Florentin Pottmeyer, Kay A. Weidenmann

Angaben zur Veröffentlichung / Publication details:

Muth, Markus, Florentin Pottmeyer, and Kay A. Weidenmann. 2020. "Failure behaviour of metal inserts embedded in CFRP subsequent to thermal, mechanical and cyclic pre-damage." *Composite Structures* 236: 111877. https://doi.org/10.1016/j.compstruct.2020.111877.

Failure behaviour of metal inserts embedded in CFRP subsequent to thermal, mechanical and cyclic pre-damage

Markus Muth[a,*], Florentin Pottmeyer[a], Kay André Weidenmann[a,b]

[a] Karlsruhe Institute of Technology (KIT), Institute for Applied Materials IAM–WK, Kaiserstr. 12, 76131 Karlsruhe, Germany
[b] Institute of Materials Resource Management (MRM), University of Augsburg (UNIA), Augsburg, Germany

ABSTRACT

One of the most efficient implementations of lightweight design is the use of carbon fibre reinforced plastics due to their outstanding specific mechanical properties. With respect to multi-material-design, carbon fibre reinforced plastic parts have to be joined to other components such as load frames or functional elements. The use of embedded metal elements, so called inserts, is favoured to avoid drilling of composites. The fibre continuity is ensured and no local bearing stresses occur. In the work at hand the influence of impact damage on the quasi-static and cyclic strength was evaluated by pre-damaging the components by various impact energies. The components show only a minor reduction of the mechanical properties for impact energies up to 12 J. For impact energies between 12 J and 16 J, a loss in the mechanical properties is evident but final failure only occurred for impact energies above 16 J.

Another aim of this study was to derive service-life-prognosis using multiple step tests and to validate these with experimentally determined S-N curves. Due to different damage mechanisms occurring under quasi-static and cyclic loads, a service-life-prognosis based on the multiple step tests was not feasible, however, a service-life-prognosis based on the experimental data is given.

1. Introduction

Lightweight structures are mainly used in the transport industry, where their outstanding specific mechanical properties help to save resources. Especially continuous fibre-reinforced, thin-walled CFRP structures have a high potential. With regard to multi-material design, the problem of the detachable connection of metallic and thin-walled fibre composites in supporting structures can be solved cost-effectively by using so-called inserts. These inserts used within the work at hand consist of a base plate with a welded-on threaded bush. With the help of inserts, it is possible to maintain fibre continuity because the drilling of the components to be connected – and thus the cutting of the supporting fibres – as is necessary with screws or rivets – can be avoided [1]. The decrease in the load-bearing capacity of the component compared to a non-drilled component is due to the stress concentration occurring at the bore [2–4].

In previous investigations, only the maximum torques and forces under quasi-static conditions have been investigated. Ferret et al. [5] dealt, for example, with two variants of a bigHead® insert under bending, tensile and compressive loads. This showed that a smaller base plate leads to an increase in tensile strength. The reason for this is the premature failure of the insert base plate.

Hopmann et al. [6] carried out pull-out tests on inserts as well as on adhesive bonded fasteners. The result of this comparison was that when using inserts, the maximum forces are about 37% higher than when using the bonded reference. The influence of manufacturing and geometry parameters on mechanical properties was investigated by Schwarz et al. [7]. Also the surface treatment of the inserts, investigated by Fleischer et al. [8], plays a decisive role. The performance of the component could be increased by up to 42% by additively applied pins on the underside of the base plate. The identification of the most critical load case for components of the type examined in this paper was determined in a separate preliminary paper [9] when considering torsion, compression, bending, tensile and shear loads. As could be shown, tensile loads are the most critical for this type of component, since it has the largest performance difference to the reference component, a bolt welded to a sheet metal. Subsequent pull-out tests showed that an increase in the base plate and/or laminate thickness results in an increase in the load bearing capacity. Another work published by the authors [10] showed by means of in-situ CT investigations that the decrease of the quasi-static forces in the pull-out test can be correlated with the detachment of the insert base plate from the lower laminate layers.

* Corresponding author.
E-mail addresses: Markus.Muth@kit.edu (M. Muth), Florentin.Pottmeyer@kit.edu (F. Pottmeyer), Kay.Weidenmann@mrm.uni-augsburg.de (K.A. Weidenmann).

As can be seen in the literature shown up to now, so far only investigations on the load bearing capacity of insert connections under quasi-static loads have been carried out. Therefore, in the following the relevant basics on the behaviour of fibre composites, especially CFRP, under cyclic, dynamic and thermal loads will be presented. By Solimen et al. [11] and Ferguson et al. [12], CFRP was investigated for the failure mechanisms under load in thickness direction. According to [11,12], the causes of component failure can be traced back to debonding, delamination and fibre/matrix cracks. In investigations by Jain et al. [13] on the fatigue strength of CFRP laminates under cyclic loading, the influence of the matrix and fibres used was considered. In addition, various influences such as previous damage, manufacturing process and type of loading have also been under investigation. According to Jain et al., damage first occurs on the micro level, which causes that stresses are redirected to undamaged areas. As a result, stiffness and strength are not influenced at first. If the load is further increased or the duration of the test continues, it is no longer possible to redirect the loads and the component fails. Helmy and Hoa [14] name matrix pockets as the starting point for delamination under cyclic loading. Matrix pockets occur, for example, when additional fibre layers or metal inserts – as in the work at hand – are inserted into simple laminates. Fong [15] describes the possibility of estimating the service life using S-N curves. What has not yet been investigated is the influence of a metallic insert embedded in the CFRP as in this paper on the cyclic properties of such hybrid components. Also, there is a lack of knowledge on the effects of impact loads introduced in advance, although these represent an important loading scenario in the later use of such a component in combination with cyclic loads. In order to determine these properties, multiple-step tests are first carried out to determine a cyclic force-displacement curve, which in turn makes it possible to make a service life prognosis [16].

A further point to be dealt with in this paper is the influence of thermal and dynamic loads as well as the mechanical pre-damage of the described components. In addition to quasi-static residual strength measurements on components pre-damaged with different energies, multiple step tests are also carried out on such components to determine the influence of mechanical damage on the cyclic properties. Such a residual strength measurement was previously performed on CFRP laminates [17,18] and sandwich panels [19,20]. Measurements by Caprino [21] showed that CFRP laminates with a pre-damage of up to 4.3 J only have a residual strength of up to 40% compared to undamaged components. By Sánchez-Sáez et al. [22] various CFRP layups were tested for their residual compressive strength after damage with a maximum of 13 J. The result was that the residual compressive strength dropped to a minimum but remained constant with a further increase of the impact energy. A 0°/90° laminate showed the worst damage tolerance. How it is also used in this work.

Since dynamic loads in the form of crash loads can also occur in the later use of such a component, such tests are also necessary in order to be able to estimate the behaviour of such a component type. The behaviour of unidirectional CFRP laminates at high strain rates was investigated by Taniguchi et al. [23]. Neither the tensile modulus nor the strength showed a longitudinal strain rate dependence. If, however, the same properties were investigated under transverse loading, both the tensile modulus and the strength increased. This behaviour can be confirmed by Harding and Welsh [24].

In addition to the tests under quasi-static and cyclic conditions and the influence of mechanical pre-damage, thermal loading of fibre composite components is also critical. Likewise, no components containing metallic load introduction elements have yet been investigated. The influence of thermal loads on the properties of CFRP was investigated by Shimokawa et al. [25], for example, and it was found that microcracks formed in the CFRP as early as 10 thermal cycles (−54 °C to 177 °C for a cycle duration of 15 min). Although the number of microcracks increased by up to 10,000 cycles, a negative influence on the residual compressive strength could not be determined.

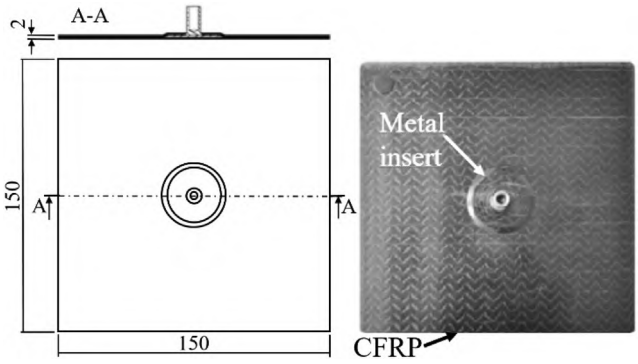

Fig. 1. Exemplary picture and dimensions of the specimen (c.f. [1]).

2. Experimental

2.1. Materials and specimen geometry

In this work the same sample geometry as in [1,8,9,26,27] was chosen to allow a comparison with previously published literature. For the component type used in this paper, the insert used, see Fig. 2, is also placed in the middle between the upper and lower CFRP layers in the middle of a CFRP plate with a thickness of 2 mm, see Fig. 1. In order to prevent the fibres from being cut during preforming, the fibres are guided around the insert bushing with the aid of a screwed-on tip. The material selected for the inserts is ANSI 304 stainless steel. The inserts consist of a round base plate and a welded on threaded bushing (Fig. 2).

The CFRP base plate of the components is impregnated with an epoxy resin (Biresin® CR170/CH150-3) from eight layers of biaxial carbon fibre pre-finished product (Hexcel NLT00 series, 0°/90°, 200 g/m^2) in the resin transfer moulding process at the Institute of Production Science (wbk) at KIT. The resulting fibre volume fraction is 44%. During infiltration, a flowmeter and mixing machine (Tartler Nodopur VS-2K) was used for mixing and dosing the resin components. The curing of the component for 60 min at 70 °C under 9 bar infiltration pressure was carried out on a hydraulic press (Lauffer type RP 400).

2.2. Test setup and procedure for quasi-static and dynamic tensile tests

The quasi-static and dynamic pull-out tests were carried out on two different testing machines depending on the test speeds to be investigated. For the test speeds of 1.5 mm/min (quasi-static test speed) and 150 mm/min, a Zwick universal testing machine was used. The test setup can be seen in Fig. 3. The load is applied via a screw that is screwed into the thread of the insert.

The clamping frame used for all tests carried out in this work, with the exception of the previous applied mechanical damage, is shown in Fig. 3. In addition, an inductive strain gauge (ISG) is installed below the specimen to measure the displacement of the laminate. For testing at higher speeds (250 mm/s and 15 m/s) a Zwick HTM5020 testing machine has been used. Here, as mentioned above, the same clamping

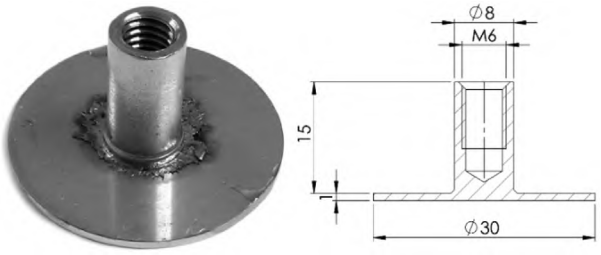

Fig. 2. Exemplary picture and dimensions of the metal insert used (c.f. [1,9,26]).

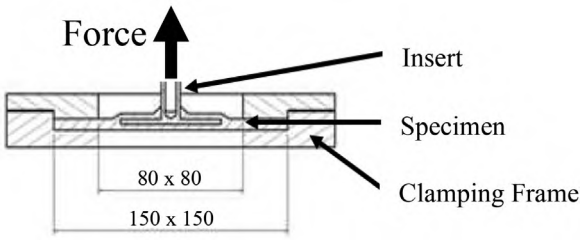

Fig. 3. Experimental fixture (c.f. [1]).

frame was used as in all other tests. The forces and displacements were measured and evaluated. The load-bearing capacity is defined as the maximum force occurring during the test. At least five specimens of each load condition were tested.

The test speed of the quasi-static tests on a Zwick universal testing machine was 1.5 mm/min. The load was introduced via a screw screwed into the insert thread. The failure criterion for the quasi-static and dynamic pull-out tests was a load drop of at least 60% of the maximum force applied.

2.3. Test setup and procedure for experiments with cyclic loading

A servo-hydraulic testing machine from Schenck was used to carry out the cyclic tests. Instead of a screw, a cylindrical shaft is clamped in the machine and screwed into the thread of the insert to introduce the load.

Since the cyclic tests are to be carried out under pure tensile load on the component, a load ratio (R) of 0.1 at a frequency of 1 Hz and a sinusoidal oscillation was selected. For the multiple-step tests, 25% of the quasi-static strength of the components was specified as the starting value. Further on, the applied maximum force was increased by 500 N after each 1500 load cycles with a constant load ratio. By analysing the force–displacement curves, cyclic force-displacement diagrams can be generated from the multiple-step tests.

In order to determine the S-N curve, 50% of the quasi-static strength as selected as initial value on the basis of these results further load levels according to ISO 13003 [29] have been chosen. The components were tested at constant force and constant load ratio until final failure.

2.4. Test setup and procedure for the pre-damaging experiments

2.4.1. Mechanical pre-damage by impact

The pre-damage of the samples for the following quasi-static and cyclic tests was performed by high speed indentations with a Instron Dynatup drop tower. The test setup is shown in Fig. 4. Following DIN EN 6038 [28], damage energies of 6, 9, 12 and 16 J were applied by varying the drop height of the impacting weight. Following the pre-damage, the residual strength under quasi-static load was determined as in Chapter 2.2.

2.4.2. Thermal pre-damage by thermal cycling

In addition to the mechanical pre-damage, thermal loads were also applied in the form of thermal cycling. The components were subjected to the temperature cycle shown in Fig. 5 for 10, 100 and 1000 times. Here, too, the residual strength was measured under quasi-static conditions as shown in Section 2.2.

3. Results

3.1. Quasi-static pull-out tests

Fig. 6 shows the force-displacement curve of a quasi-static (1.5 mm/min) tested example component (black). Simultaneously the deflection of the CFRP underside is shown. Up to a deflection of 4.5 mm, a linear

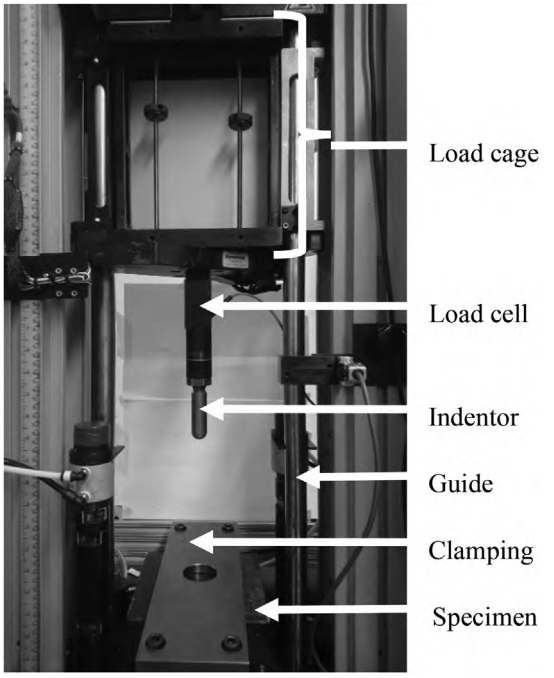

Fig. 4. Test setup for the pre-damage by impact.

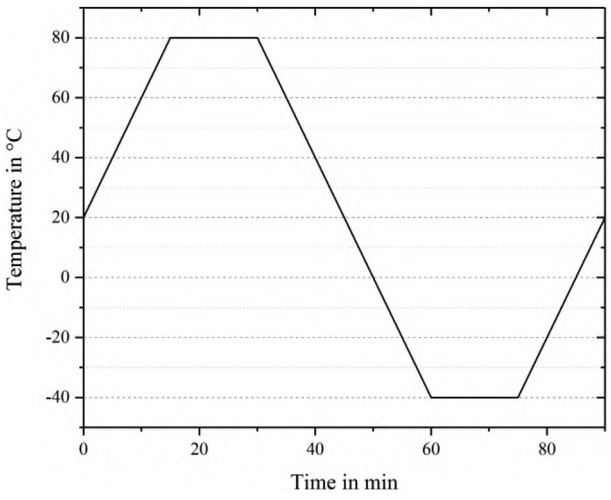

Fig. 5. temperature during one cycle.

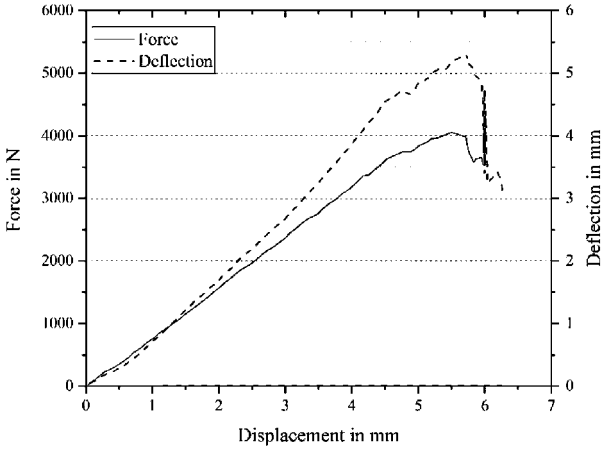

Fig. 6. Force-/displacement-diagram of a specimen tested at 1.5 mm/min.

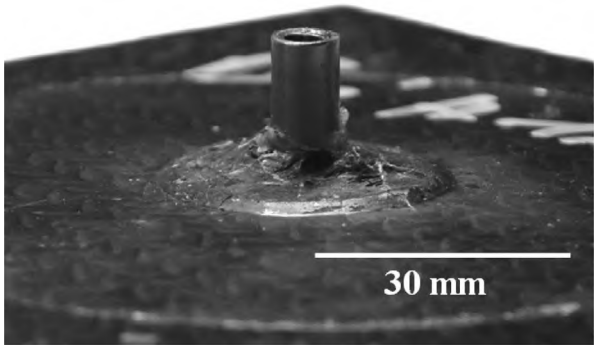

Fig. 7. Failure modes of the specimen types after the quasi-static tests.

increase of the deflection can be seen, which corresponds exactly to the displacement of the testing machine. From 4.5 mm or a force of 3800 N, however, the deflection increases less than the crosshead displacement dose. Similarly, a small plateau in the deflection can also be seen in the first significant drop in force at approx. 4000 N. This behaviour continues with the following force drops up to the final failure.

Fig. 7 shows the image of a failed component with the typical cross-shaped cracks [9] around the inserts bushing.

Table 1 summarises the results of the individual tests.

3.2. Dynamic pull-out test

As already shown in Fig. 6, Fig. 8 shows the force-displacement curve of an example component at a test speed of 150 mm/min and the deflection against the displacement of the crosshead. The deflection and also the force at approx. 5.5 mm crosshead displacement show a clear decrease which is to be regarded as the actual failure point of the component. What clearly noticeable is that until the complete failure at 5.5 mm crosshead displacement no single small drops in the deflection or force can be seen.

Fig. 9 shows the picture of a component after its failure. Instead of single fibre breaks, failure of fibre bundles can be seen.

The tests shown so far were carried out on a universal testing machine with a maximum test speed which is too low for the higher speeds to be tested. Therefore, the tests were carried out with higher test speeds of 250 mm/s and 15 m/s on a machine with a different machine stiffness and no possibility to measure the deflection directly on the component. Thus a direct comparison of the component stiffness is not possible. In all tests with traverse displacements of 250 mm/s or higher, the insert was pulled out of the laminate, leading to complete failure of the components. An exemplary curve shape of the recorded force-displacement curves of a test with a test speed of 250 mm/s is shown in Fig. 10. As can be seen, the vibrations in the test setup generated during the test at high speeds interfere with the force actually measured by the load cell, which in turn hinders a statement from being made about the total energy absorbed. The final failure occurs at approximately 5000 N and a displacement of 6 mm.

The highest possible test speed was 15 m/s, which therefore also represents the highest test speed examined in this paper. Fig. 11 shows

Table 1
Quasi-static pull-out test results (s_{max} maximum displacement, a. v. average value, st. dev. standard deviation).

Specimen no.	s_{max} in mm	F_{max} in N
1	6.37	4162
2	6.24	4426
3	7.12	4868
4	6.92	4333
5	6.91	4502
Average	6.71 ± 0.39	4458 ± 262

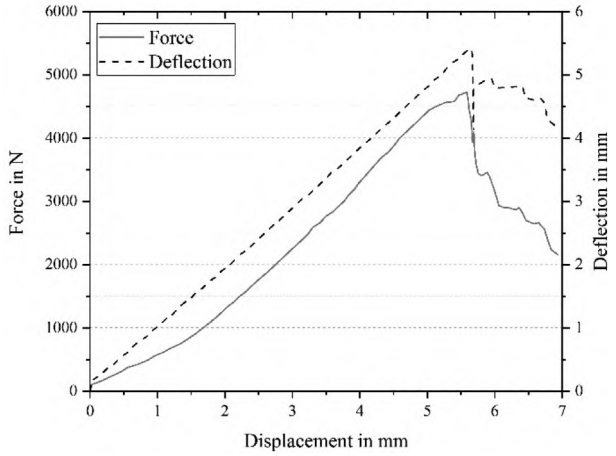

Fig. 8. Force-/displacement-diagram of a specimen tested at 150 mm/min.

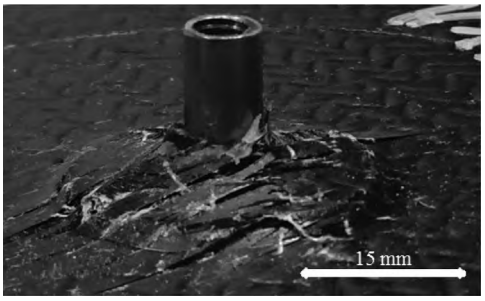

Fig. 9. Post-mortem picture of a specimen tested with 150 mm/min.

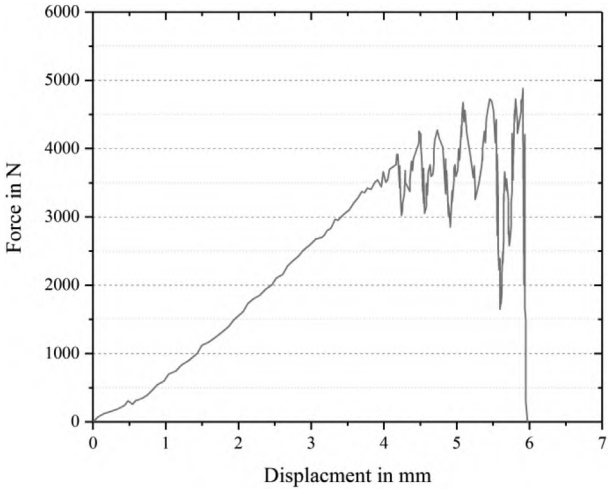

Fig. 10. Force-/displacement-diagram of a specimen tested with 250 mm/s.

an example of the recorded force-displacement curves. The oscillations in the test setup that occurred during the tests with a lower test speed and lead to an incorrect measurement of the load cell did not occur during these tests.

Failure of the components at test speeds above 250 mm/s occurs by delaminating the CFRP plate and pulling the insert completely out of the CFRP. Which differs is the degree of deformation of the insert base plate, as shown in Fig. 12.

As can be seen in Fig. 13, up to a test speed of 250 mm/s the maximum force absorbed in the test increases only slightly. Only at the highest possible test speed of 15 m/s there is a significant increase in the force, which is also accompanied by an increase in the standard deviation of the results.

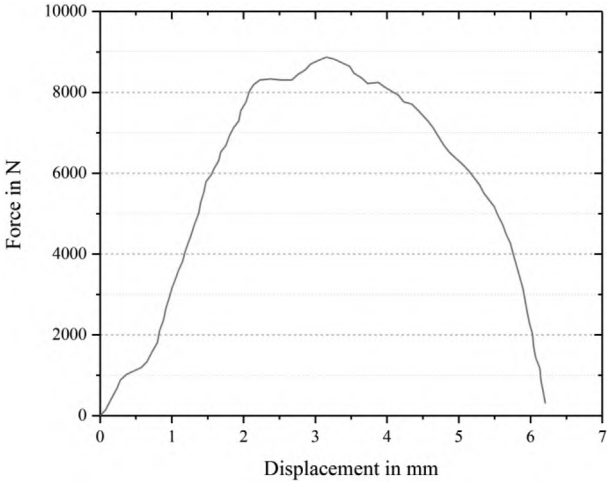

Fig. 11. Force-/displacement-diagram of a specimen tested with 15 m/s.

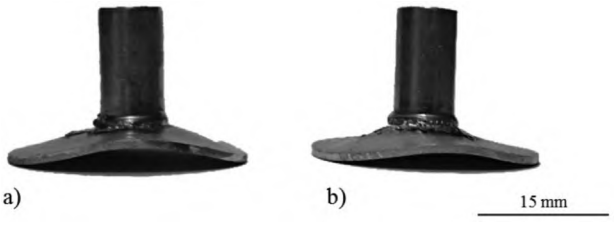

Fig. 12. Post-mortem picture of the deformed inserts with a) 250 mm/s and b) 15 m/s.

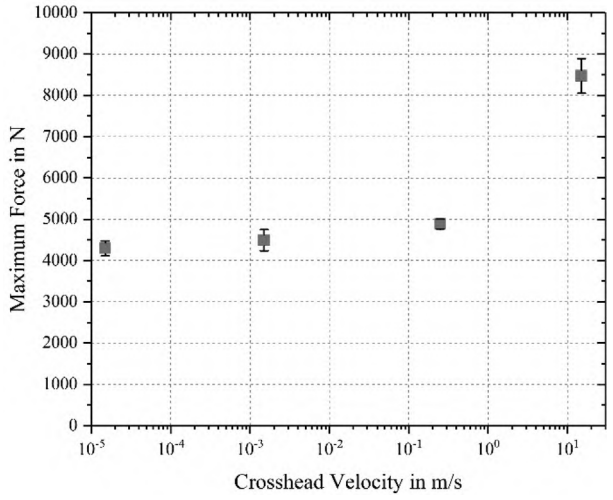

Fig. 13. Load bearing capacities of all deformation rates.

3.3. Residual strength of mechanical pre-damaged specimens

The mechanical pre-damage of the components caused the damages shown in Fig. 14, which depends on the impact energy applied. If the components were pre-damaged with 6 J, there was no damage to the laminate at the point of impact. Another picture can be seen on the actual upper side of the laminate, where the typical cross-shaped cracks around the insert bushing described in [27] occurred. When looking at the x-ray computed tomographs (CT) images (cf. Fig. 14a) of the component, cracks in the laminate directly in the area of the impact point and a deformation of the insert base plate were also visible. From an impact energy of 9 J, in addition to the damage described above, external cracks also occurred in the laminate in the area of the impact

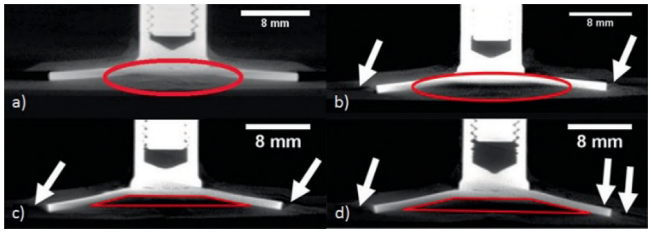

Fig. 14. CT-scans of the pre-damaged specimens with marked cracks at the edge of the base plate (white arrows) and defects at the interface between the insert and the CFRP laminate (in the marked areas) a) 6 J impact energy b) 9 J impact energy c) 12 J impact energy d) 16 J impact energy (c.f. [27]).

point and CT images (cf. Fig. 14b) showed that the insert base plate is not only deformed more, but also detached from the laminate. In the laminate, in addition to the delamination under the insert, delamination also occurred in the edge area of the insert base plate. With a further increase of the impact energy (12 J and 16 J) no further damage type appeared, only the degree of damage increased further (Fig. 14c and d).

In addition to the damage in the laminate, the impact at increased impact energies also leads to defects on the surface of the laminate (cf. Fig. 15). In addition to the cross-shaped cracks described in [27] on the upper side of the component, increasing impact energy also leads to damage of the underside of the component by the indentor.

The residual strength of the components after mechanical pre-damage by impact was determined under quasi-static conditions. Fig. 16 shows the results of the tests. As can be seen there, the influence of the previous damage on quasi-static properties of the components up to an impact energy of 12 J is only slight. The determined mean values of the component strength remain in the range of the undamaged components, whereas the variance of the strength tends to increase towards higher energies. Only from an impact energy of 16 J is a reduction of the average component strength by approx. 50% to be observed. The failure mode of the components does not differ in any of the cases from that of an undamaged component (cf. Fig. 7).

3.4. Residual strength of thermal loaded specimens

As described in chapter 2.4, the components were exposed to 10, 100 or 1000 temperature cycles (see Fig. 5) before measuring the residual strength. The residual strength was then tested under quasi-static conditions. The principal shape of the recorded force-displacement curves (cf. Fig. 6) and the damage pattern (cf. Fig. 7) after completion of the test do not differ from that of non-cycled components. The load

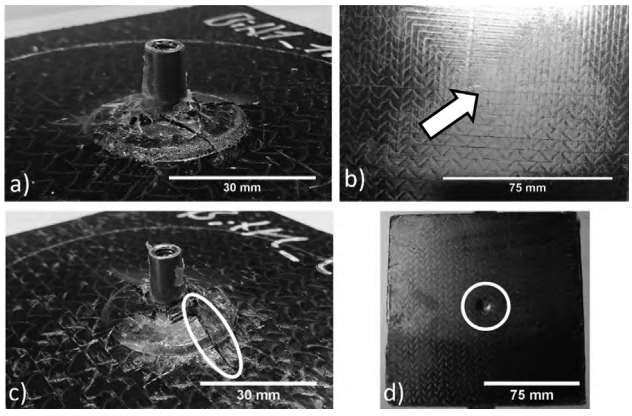

Fig. 15. a) Failure at the upper side of a specimen pre-damaged by 6 J b) failure at the lower side of a specimen pre-damaged by 6 J c) failure at the upper side of a specimen pre-damaged by 16 J (crack is marked) d) failure at the lower side of a specimen pre-damaged by 9 J (marked surface damages).

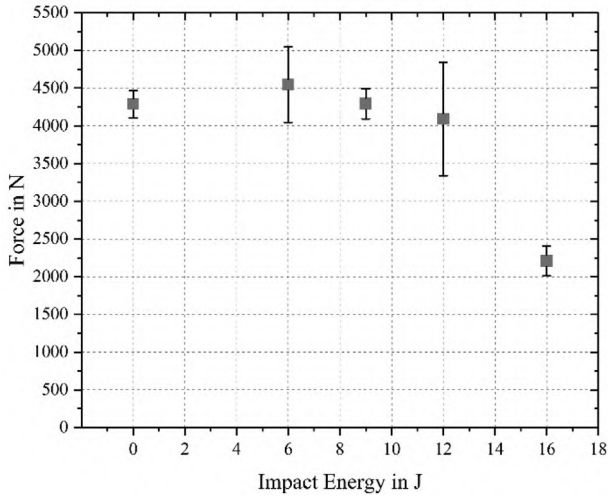

Fig. 16. Load bearing capacities related on the impact energy.

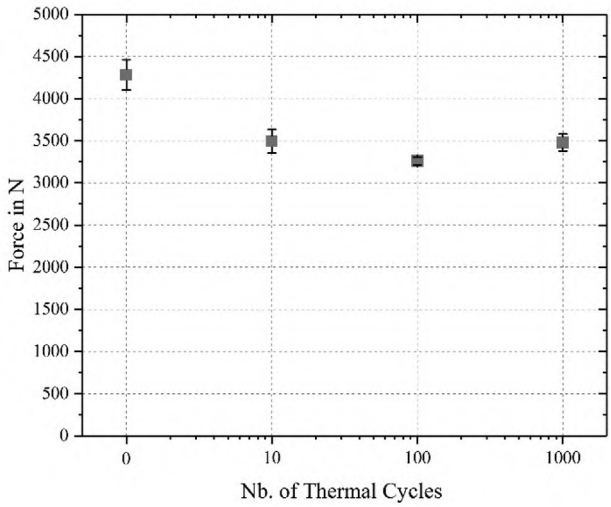

Fig. 17. Load bearing capacities of all performed number of thermal.

bearing capacity as a function of the number of temperature cycles is shown in Fig. 17. As can be seen, the load bearing capacity of the components decreases significantly after only 10 temperature cycles, but remains constant with a further increase in the number of cycles.

3.5. Multiple step tests

An exemplary force-displacement curve is shown in Fig. 18. The tests were started at a maximum force of 1115 N and after each 1500 load cycles, the load was increased by 500 N. Within the first two load stages no increase of the displacement difference between the upper and lower dead centre of the applied sinusoidal oscillation can be seen. From the third load stage onwards, the displacement at the two dead centres increases slightly and significantly from the fourth load stage onwards. In the test shown, failure occurred within the fifth load stage, which can also be seen from the displacements increasing significantly more strongly than before at the beginning of the load stage. The basic behaviour of the tested components with and without mechanical pre-damage does not differ.

A clear difference to the failure of the components can be seen in the type of failure. The components fail under cyclic conditions not due to delamination but due to a fracture of the insert base plate around the bushing socket. Fig. 19 shows CT scans of a failed component without prior mechanical damage directly in the area of the failed baseplate. It

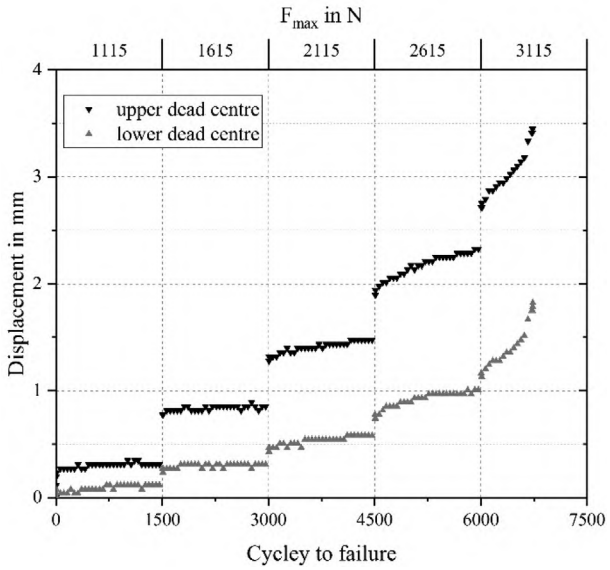

Fig. 18. Characteristic displacement-number of cycle pattern for the components tested.

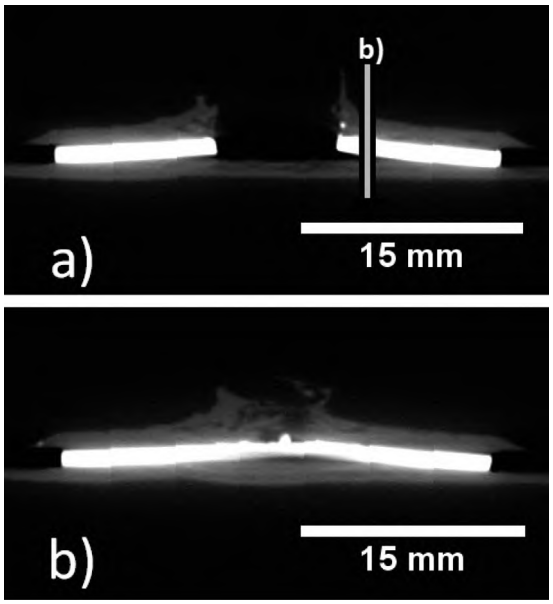

Fig. 19. CT-scan of a failed specimen) cross-section in the middle of the inserts base plate b) cross-section at the position marked in a).

can be clearly seen that the remains of the insert base plate are still in the laminate and only minimal delamination can be detected (Fig. 19b).

If one now considers not only the failure of the components that have not been pre-damaged but also the influences of the mechanical pre-damage on the cyclic properties in the multiple-step test, the failure pattern of the components changes with increasing damage. At 6 J pre-damage energy, there is no change in the type of failure. Only after 9 J impact energy does the failure of the components partly occur by pulling the insert out of the laminate, but there are also components that fail according to the previously observed failure mode. A mixture of the two types of failure also occurred, as can be seen in Fig. 20.

From an impact energy of 12 J, only mixed failure or failure due to an insert pulled out of the laminate occurred, as in the quasi-static and dynamic tests. With a further increase in the pre-damage energy to 16 J, only failure due to an insert pulled out of the laminate could be observed in the multiple-step tests. As can be seen in Table 2, the

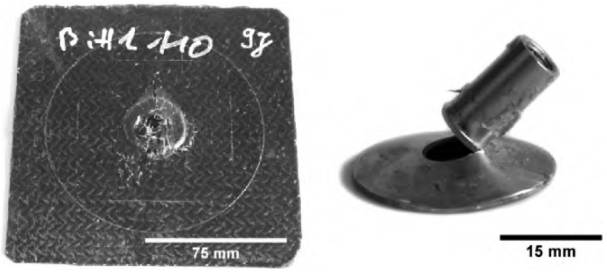

Fig. 20. Example of a mixed mode failure of specimens pre-damaged at 9 J.

Table 2
Summarized multiple step test results.

Specimen	Cycles to failure	F_{max} in N
0J	6216 ± 300	3091 ± 57
6J	6078 ± 134	3148 ± 58
9J	6229 ± 392	2910 ± 267
12J	6430 ± 1402	3148 ± 479
16J	5356 ± 1252	2880 ± 346

maximum applied load changes only slightly with increasing pre-damage energy, whereas the standard deviation of the results increases significantly.

3.6. S-N curves

In order to determine S-N curves, in addition to the multiple-step tests, cyclic tests were also carried out at constant maximum force. The initial value for the first cyclic tests was 50% of the quasi-static strength and the following load levels were defined on the basis of these results. The test parameters resulting from this procedure are shown in Table 3. From a cycle number of $1*10^6$ cycles on, the tested components were defined as run-throughs.

Fig. 21 shows the S-N curve determined in this way. This curve has a special feature, because not as usual the induced stresses, but the induced forces were plotted against the maximum number of load cycles of the individual tests. The reason for this is that no stress or strain could be defined as in coupon tests. As can be seen in Fig. 21, the expected linear relationship between the force and the logarithmic number of load cycles results for the tested components.

Fig. 22 shows a CT scan of a run-trough component. It can be seen that neither the insert nor the laminate has been damaged in this component. The components which were tested at higher loads fail again in the same way as the undamaged components in the multiple-step test.

4. Discussion

4.1. Dynamic pull-out test

In the case of components tested at 1.5 mm/min and 150 mm/min, it is possible to compare the deflection of the underside of the component due to the inductive strain gauge used (see Fig. 6 (1.5 mm/min)

Table 3
Load levels and test results of the single-step tests (% quasist. means percent of the quasi-static strength).

Load level	% Quasist.	$F_{experiment}$ in N
1	10	446
2	25	1115
3	35	1560
4	50	2230

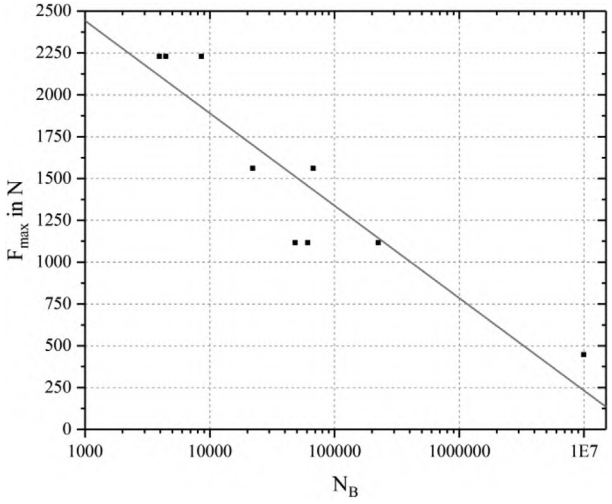

Fig. 21. S-N curve for the tested specimens.

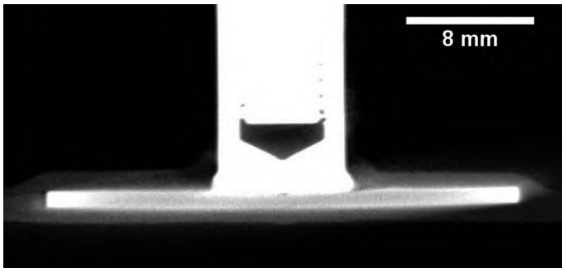

Fig. 22. CT-scan of an endured specimens after single-step test (F_{max} = 446 N).

and Fig. 8 (150 mm/min)). At a test speed of 1.5 mm/min, the curve of the ISG initially flattens out at a deflection of more than 4.5 mm, indicating a relative movement between the insert underside and the laminate underside. From this it can be seen that the insert underside first detaches from the laminate before the total failure of the component occurs. The components tested at 150 mm/min, on the other hand, only show an abrupt collapse during deflection when the component fails, which in turn suggests that the insert underside has only abruptly detached itself from the laminate prior to total failure. The assumptions described also allow the conclusion that the strength of the insert/laminate interface depends strongly on the test speed.

A difference in the failure of the components can also be seen in the fact that at higher test speeds fibre bundle failures are observed instead of single fibre failure occurring under quasi-static conditions (cf. Fig. 7). The abrupt failure of the insert/laminate interface towards higher test speeds is also responsible for this behaviour. This can also be seen in Fig. 12. Here it becomes clear that the plastic deformation of the insert decreases steadily at higher test speeds. Here, too, the increasing strength of the insert/laminate interface at higher test speeds is to be regarded as the cause.

In contrast to CFRP, the pure matrix strength depends on the strain rate [23,24,30]. Taniguchi et al. [23] investigated the properties, especially the tensile strength, transverse to the loading direction. Strain rates from $1.04*10^{-4}$ 1/s to 100 1/s corresponding to a test speed of 0.156 mm/min and 2.5 m/s were investigated. Between these test speeds, the authors were able to determine a linear increase of the tensile strength by approx. 18%, which in turn confirms the strain rate dependence of the matrix strength. In Fig. 13 it can be seen that the load-bearing capacity increases linearly by approx. 14% at test speeds of up to 250 mm/s. This is confirmed by the strain rate dependence of the matrix strength. In the present study an epoxy resin was used as matrix and the determined value shows a good quantitative agreement with the literature values. Only at a test speed of 15 m/s does the

strength increase abruptly by approx. 100% compared to the quasi-static speed of 1.5 mm/min and cannot be confirmed with literature values.

4.2. Residual strength of thermal and mechanical pre-damaged specimens

Fig. 17 summarizes the results of the quasi-static residual strength measurements for the thermally cycled components. Looking at the results, it becomes clear that 10 temperature cycles are sufficient to reduce the residual strength of the components by approx. 20%. However, it is also noticeable that the residual strength does not decrease further after these 10 cycles. Basically, residual stresses always occur in CFRP laminates due to the different shrinkage of fibre and matrix during the cooling process after curing of the matrix. An even higher discrepancy of the coefficients of thermal expansion can be found with CFRP metal hybrid components. As a result, the residual stresses in such components are even more pronounced than in pure CFRP components [31–33]. According to [34] and [35], the residual stresses generated during production are sufficient to produce matrix cracks. If, due to thermal cycling, the difference between the stress-free temperature, which can be compared with the curing temperature [36–38], and the operating temperature increases, the level of the residual stresses increases further [39,40]. The number of microcracks and the residual strength of thermally loaded CFRP laminates was investigated by Shimokawa et al. [25]. Microcracks and the reason for the increased residual stresses in the matrix were found within the first ten temperature cycles. A further deterioration of the determined residual strengths could not be determined with increasing number of temperature cycles, although the number of microcracks increased. The increase in the number of microcracks with increasing number of temperature cycles is also confirmed by Ju and Morgan [39]. As can be seen in Fig. 5, the lowest temperature during the temperature cycles is −40 °C. This leads to further increase in residual stresses which result in microcracks in the interface between CFRP and insert. The expected increasing number of microcracks with increasing number of temperature cycles after [25] had no influence on the residual strength of the components. Also the variance of the results did not increase with increasing number of temperature cycles.

The measured residual strengths of the pre-damaged components can be seen in Fig. 16. What is particularly striking here is that up to an impact energy of 12 J no loss of mechanical properties occurs although both the insert/laminate interface and the insert itself are damaged or have deformed (cf. Fig. 14). In addition to the damage to the insert and the interface caused by the impact, cracks in the laminate at the edge of the insert base plate became increasingly apparent with increasing impact energy. From an impact energy of 16 J, the measured residual strength decreases on average by approx. 50%. If one compares the results obtained with the literature, it can be seen that the residual strengths determined are significantly higher compared to [21] Due to the previous damage caused by impact, a reduction of the residual strength by approx. 60% was determined here from energies of 4.3 J and above. In addition to the mean values for the residual strength, the scattering of the values should also be considered. This shows that the mechanical pre-damage does indeed have an influence on the results, as these scatter significantly more with increasing impact energy and the probability of early failure is thus significantly increased in comparison to undamaged components.

4.3. Influence of the impact on the multiple step tests

As already described above, as the impact energy increases, the amount of damage occurring in the laminate also increases (see Fig. 8MM). As described in [27], this also leads to greater damage at the insert/laminate interface. In addition to the damage already present in the laminate before the tests, delamination becomes increasingly critical for failure in the edge area of the insert base plate. Chapter 3.5 describes the different failure modes that occur, which are summarized again in Table 4.

Table 4
Failure modes of the components tested after the multiple step tests.

Impact energy in J	Failure mode			
	Fracture of the base plate	Insert pulled out:		Mixed mode
		With further deformation	No further deformation	
Juvenile	X			
6	X			
9	X	X		X
12		X		X
16			X	

The reason for the same failure mode for undamaged components and those pre-damaged with 6 J can be found in the fact that for both component types there is no damage to the laminate at the base plate edges, nor was the interface between laminate and insert damaged. With increasing damage of the described interface at higher impact energies, the failure mode also changes. The different damage modes available at 9 J impact energy indicate that not all tested components have the same degree of interfacial damage. A further criterion which favours the removal of the insert from the laminate is the damage caused to the upper side of the laminate by the impact test. This is to be compared with the failure patterns occurring in the quasi-static tests. Only at damage energies of 12 J and above the complete failure of the insert base plate ceases. Above this energy, only mixed failure or an insert pull-out occurs. This can be explained by the fact that, due to the even more severely damaged interface, the loads on the matrix in the thickness direction have increased significantly, which can also be seen from the cracks on the laminate surface that appear more clearly (Fig. 15) [11,12]. Furthermore, the deformation of the insert base plate can also be seen in this series of tests, as shown in Fig. 14, is significantly greater than in the previous energies. The matrix pockets described by Helmy [14] at the edges of the insert baseplates appear to have an influence on the failure pattern only if the interface is already damaged and the pockets then act as a starting point for cracks in the laminate. From an impact energy of 16 J, only one failure mechanism could be observed. From this energy on, only the inserts are pulled out of the laminate, whereby their base plate no longer deforms plastically. The reason for this behaviour is the boundary surface which is not existing anymore caused by the impact with high energies and the strong damage of the laminate on the lower and upper side which could counteract the removal of the insert. Fig. 23 summarizes the results of the quasi-static test of an undamaged component and the results of the multiple-step tests.

It can be seen that the cyclic strength of undamaged components in the multiple-step test is approx. 30% lower than the strength in quasi-static conditions. This is primarily due to the fact that the failure modes of the two test types differ fundamentally. In the case of quasi-static loads, the separation of the interface between the insert base plate and the laminate is critical for failure. The resulting delamination is based on the increased matrix load at external loads in component thickness direction [11,12]. In undamaged specimens and specimens damaged with 6 J, failure of the insert occurs under cyclic conditions due to the notch effect in the transition from the insert bushing to the base plate. The samples pre-damaged with energies from 9 J on show increased failure under cyclic load due to delamination, starting from the edge of the insert base plate which is further promoted under cyclic conditions. Here again the increased load on the matrix mentioned in [11,12] as well as the matrix pockets described by Helmy [14] at the edge of the insert baseplate play a decisive role. The initially increased variance of the strengths at 12 J impact energy is due to the stronger damage in the

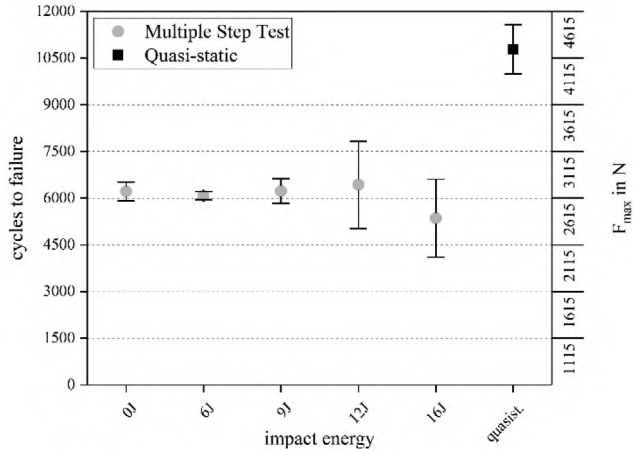

Fig. 23. Comparison between the quasi-static strength and the strength in multiple step tests for non- and pre-damaged specimens.

laminate compared to the samples damaged by 9 J (see Fig. 14). The reasons for the drop in strength at 16 J impact energy are the completely detached boundary layer and the even stronger delamination in the edge area of the base plate. The results shown suggest that the two failure modes shown require similarly high energies for triggering, which also explains the good damage tolerance of this component type.

4.4. Lifetime prediction

When determining the service life (failure of the component after a certain number of load cycles (N_B)) of composite materials according to Manson [41] and Coffin [42], the problem of determining values for the plastic strain amplitude arises. According to Basquin [43], however, a correlation between the stress amplitude and N_B can be established; this is shown in Eq. (1).

$$\frac{\Delta\sigma}{2} = \sigma_B^{'} \cdot (N_B)^b \tag{1}$$

By quasi-static tensile tests $\sigma_B^{'}$ can be determined according to [44]. The service life described by equation (2) can be estimated according to [16] by determining a cyclic stress-strain curve.

$$\sigma_S = k^{'} \cdot (\varepsilon_{p,S})^{n^{'}} \tag{2}$$

In addition, a relationship between b and n' can be established by Eq. (3).

$$b = -\frac{n^{'}}{1 + 5n^{'}} \tag{3}$$

From the relationships resulting from Eqs. (1)–(3), it is therefore possible to empirically estimate a lifetime prognosis for the components shown. A special feature of this work is that no stresses and strains can be determined in the tests performed, but only the force and displacement amplitude is obtained.1 Therefore, the described parameters are determined from a cyclic force-displacement curve. The parameters b, n′ and $\sigma_B^{'}$ resulting from the equations are used as b_F, $n_F^{'}$ and $\sigma_{B,F}^{'}$ in the following. The fatigue strength exponent b_F is determined from $n_F^{'}$, which in turn was determined from the slope of the cyclic force-displacement curve. The maximum force resulting in the tests performed is finally described by $\sigma_{B,F}^{'}$.

To estimate the service life of the tested components, the parameters shown in Table 5 were determined using Eqs. (1)–(3) under the limitations shown.

The estimation of the lifetime for different load levels resulting from the values summarized in Table 5 is listed in Table 6.

It can be seen that the service life of the investigated components is overestimated by approximately two orders of magnitude with the selected method, regardless of the selected load horizon. The reason for this lies in the fundamentally different failure modes in quasi-static, multiple-step and cyclic tests. An estimation of the service life according to Basquin is, however, possible directly on the basis of the experimental data, as Fig. 24 shows.

The estimation of the lifetime according to Basquin [43] resulting from the experiments is possible with Eq. (4).

$$\frac{\Delta\sigma}{2} = 372,5MPa \cdot (N_B)^{-0,26} \tag{4}$$

Table 5
Calculated parameters.

Parameter	Value
$n_F^{'}$	0.3225
b_F	−0.1234
$\sigma_{B,F}^{'}$	4458 N

Table 6
Comparison of forecast and experimental data.

		Cycles to failure	
% quasi-static	ΔF in N	Basquin Morrow	Experimental data
10	402	$8.1*10^{10}$	$1.0*10^{6}$
25	1004	$4.8*10^{7}$	$1.1*10^{5}$
35	1404	$3.2*10^{6}$	$3.8*10^{4}$
50	2008	$1.8*10^{5}$	$5.7*10^{3}$

5. Summary and conclusions

The influence of various loads such as thermal and mechanical predamage as well as dynamic and cyclic conditions on the mechanical properties in the pull-out test, the critical load case determined by [9], was investigated. In the dynamic tests initially carried out at increased crosshead speeds, it was shown that the loading capacity of the tested components depends strongly on the loading speed. When the load speed is increased to 15 m/s based on quasi-static conditions, the recorded maximum forces show an increase of up to 100%. The degree of laminate damage also increases, whereas the deformation of the insert decreases with increasing loading speed. The reason for this is the behaviour of the interface between the insert and the laminate. At low loading speeds, this interface gradually fails, whereas at high loading

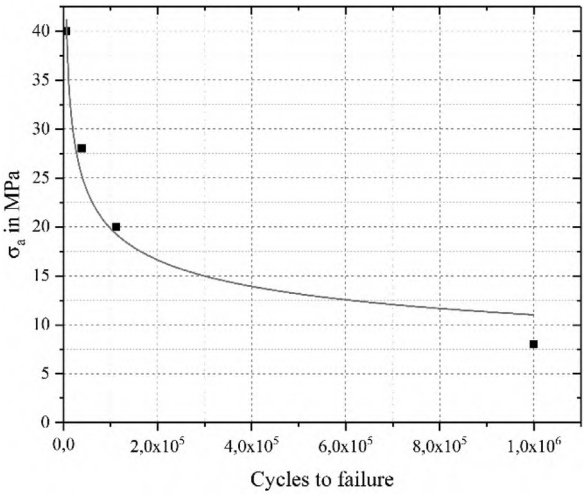

Fig. 24. lifetime estimation on the basis of the experimental data.

speeds it fails abruptly. To check the thermal influences on the load bearing capacity of such a hybrid component, components were first subjected to the temperature cycle shown in Fig. 5 for 10, 100 and 1000 cycles. In subsequent quasi-static residual strength measurements, it was determined that the residual strength had already decreased by approx. 20% after 10 cycles, but that it would not decrease further with a higher number of cycles. The reason for the residual strength not decreasing further could not be clarified beyond doubt. It is generally described in the literature that thermal cycling causes microcracks at the interface between insert and laminate, the density of which should increase with increasing number of temperature cycles. This behaviour will be investigated in future projects. In addition to residual strength measurements on thermally damaged components, residual strength measurements were also carried out on mechanically damaged components due to impact. Impact energies of 6 J, 9 J, 12 J and 16 J were investigated. In these measurements, the residual strength did not decrease significantly at up to 12 J. This was surprising as both the laminate and the insert showed obvious damage at these energies. A significant decrease of the residual strength was only observed at an impact energy of 16 J and above. It is not possible to estimate the service life without complex simulations, since the basic mechanisms responsible for the failure of the components differ in cyclic and quasi-static load cases.

Data availability statement

The raw and processed data required to reproduce these findings cannot be shared at this time due to technical or time limitations.

Declaration of Competing Interest

The authors declare that they have no known competing financial interests or personal relationships that could have appeared to influence the work reported in this paper.

Acknowledgements

This paper is based on investigations of the subproject 3 –"Fundamental research of intrinsically produced FRP-/metal-composites – from embedded insert to load bearing hybrid structure" – of the priority program 1712 "Intrinsic hybrid composites for lightweight load-bearings", which is kindly supported by the German Research Foundation (DFG). The authors kindly acknowledge the Institute for Production Science (wbk) of KIT for the manufacturing of the specimens within the cooperation in the abovementioned subproject.

Appendix A. Supplementary data

Supplementary data to this article can be found online at https://doi.org/10.1016/j.compstruct.2020.111877.

References

[1] Gebhardt J, Fleischer J. Experimental investigation and performance enhancement of inserts in composite parts. Procedia CIRP 2014;23:7–12.
[2] Kolesnikov B, Herbeck L, Fink A. CFRP/titanium hybrid material for improving composite bolted joints. Compos Struct 2008;83(4):368–80.
[3] Xiao Y, Ishikawa T. Bearing strength and failure behavior of bolted composite joints (part I: Experimental investigation). Compos Sci Technol 2005;65(7):1022–31.
[4] Eriksson I. On the bearing strength of bolted graphite/epoxy laminates. J Compos Mater 1990;24(12):1246–69.
[5] Ferret B, Anduze M, Nardari C. Metal inserts in structural composite materials manufactured by RTM. Compos A Appl Sci Manuf 1998;29(5–6):693–700.
[6] Hopmann C, Fecher ML, Lineman L, Bastian R, Gries T, Schnabel A, et al. Comparison of the properties of Onserts and Inserts for a high volume production of structural composite parts. J Plastics Technol 2013;9(4):179–206.
[7] Schwarz M, Magin M, Peil C, Schurmann H. Thin-walled FRP-laminates and local bending moments-incompatible or solvable by a skillful design. Int Tagung Verstärkte Kunststoffe Duroplast Formmasse 2004;28:29.
[8] Fleischer J, Gebhardt J. Experimental investigation of metal inserts embedded in composite parts manufactured by the RTM process. In: 13th Japan International SAMPE Symposium and Exhibition, Nagoya, Japan; 2013.
[9] Gebhardt J, Pottmeyer F, Fleischer J, Weidenmann K. Characterization of metal inserts embedded in carbon fiber reinforced plastics. Mater Sci Forum 2015.
[10] Pottmeyer F, Bittner J, Pinter P, Weidenmann KA. In-situ CT damage analysis of metal inserts embedded in carbon fiber-reinforced plastics. Exp Mech 2017;57(9):1411–22.
[11] Soliman E, Al-Haik M, Taha MR. On and off-axis tension behavior of fiber reinforced polymer composites incorporating multi-walled carbon nanotubes. J Compos Mater 2012;46(14):1661–75.
[12] Ferguson RF, Hinton MJ, Hiley MJ. Determining the through-thickness properties of FRP materials. Compos Sci Technol 1998;58(9):1411–20.
[13] Jain A, Hack M, Verpoest I, Lomov S, van Paepegem W, Seyfarth J. Betriebsfestigkeitsbewertung von Faserverbundwerkstoffen. In: 39. Tagung DVM-Arbeitskreis Betriebsfestigkeit:'Werkstoffe und Fügeverfahren: Neue Herausforderungen für die Betriebsfestigkeit'; 2012, p. 1–16.
[14] Helmy S, Hoa SV. Tensile fatigue behavior of tapered glass fiber reinforced epoxy composites containing nanoclay. Compos Sci Technol 2014;102:10–9.
[15] Fong JT. What is fatigue damage? Damage in composite materials: basic mechanisms, accumulation, tolerance, and characterization. ASTM International; 1982.
[16] Morrow J. Cyclic plastic strain energy and fatigue of metals. Internal friction, damping, and cyclic plasticity. ASTM International; 1965.
[17] Ishai O, Shragai A. Effect of impact loading on damage and residual compressive strength of CFRP laminated beams. Compos Struct 1990;14(4):319–37.
[18] Hawyes VJ, Curtis PT, Soutis C. Effect of impact damage on the compressive response of composite laminates. Compos A Appl Sci Manuf 2001;32(9):1263–70.
[19] Caprino G, Teti R. Impact and post-impact behavior of foam core sandwich structures. Compos Struct 1994;29(1):47–55.
[20] Wang B, Wu L-Z, Ma L, Feng J-C. Low-velocity impact characteristics and residual tensile strength of carbon fiber composite lattice core sandwich structures. Compos B Eng 2011;42(4):891–7.
[21] Caprino G. Residual strength prediction of impacted CFRP laminates. J Compos Mater 1984;18(6):508–18.
[22] Sánchez-Sáez S, Barbero E, Navarro C. Compressive residual strength at low temperatures of composite laminates subjected to low-velocity impacts. Compos Struct 2008;85(3):226–32.
[23] Taniguchi N, Nishiwaki T, Kawada H. Tensile strength of unidirectional CFRP laminate under high strain rate. Adv Compos Mater 2007;16(2):167–80.
[24] Harding J, Welsh LM. A tensile testing technique for fibre-reinforced composites at impact rates of strain. J Mater Sci 1983;18(6):1810–26.
[25] Shimokawa T, Katoh H, Hamaguchi Y, Sanbongi S, Mizuno H, Nakamura H, et al. Effect of thermal cycling on microcracking and strength degradation of high-temperature polymer composite materials for use in next-generation SST structures. J Compos Mater 2002;36(7):885–95.
[26] Wilkening J, Pottmeyer F, Weidenmann KA. Research on the interfering effect of metal inserts in carbon fiber reinforced plastics manufactured by the RTM process. In: 17th European Conference on Composite Materials, Munich, Germany; 2016.
[27] Pottmeyer F, Weispfenning M, Weidenmann KA. Research of the load bearing capacity of inserts embedded in CFRP under different loading conditions. World Acad Sc Eng Technol Intl J Chem Mol Nucl Mater Metall Eng 2016;11(1):1–8.
[28] DIN German Institute for Standardization. Aerospace series – fibre reinforced plastics – test method – determination of the compression strength after impact; 49.025.40(DIN EN 6038). Berlin: Beuth Verlag GmbH; 2016.
[29] International Organization for Standardization. Fibre-reinforced plastics – Determination of fatigue properties under cyclic loading conditions;83.120(13003); 2003.
[30] Miyano Y, Nakada M, Kudoh H, Muki R. Prediction of tensile fatigue life under temperature environment for unidirectional CFRP. Adv Compos Mater 1999;8(3):235–46.
[31] Kim HS, Park SW, et al. Smart cure cycle with cooling and reheating for co-cure bonded steel/carbon epoxy composite hybrid structures for reducing thermal residual stress. Compos A Appl Sci Manuf 2006;37(10):1708–21.
[32] Shin KC, Lee JJ. Effects of thermal residual stresses on failure of co-cured lap joints with steel and carbon fiber-epoxy composite adherends under static and fatigue tensile loads. Compos A Appl Sci Manuf 2006;37(3):476–87.
[33] Parlevliet PP, Bersee HEN, Beukers A. Residual stresses in thermoplastic composites—a study of the literature—Part I: formation of residual stresses. Compos A Appl Sci Manuf 2006;37(11):1847–57.
[34] Timmerman JF, Tillman MS, Hayes BS, Seferis JC. Matrix and fiber influences on the cryogenic microcracking of carbon fiber/epoxy composites. Compos A Appl Sci Manuf 2002;33(3):323–9.
[35] Bogetti TA, Gillespie Jr JW. Process-induced stress and deformation in thick-section thermoset composite laminates. J Compos Mater 1992;26(5):626–60.
[36] Yu Y, Ashcroft IA, Swallowe G. An experimental investigation of residual stresses in an epoxy-steel laminate. Int J Adhes Adhes 2006;26(7):511–9.
[37] Jumbo FS, Ashcroft IA, Crocombe AD, Wahab MA. Thermal residual stress analysis of epoxy bi-material laminates and bonded joints. Int J Adhes Adhes 2010;30(7):523–38.
[38] Hart-Smith LJ. Adhesive-bonded single-lap joints. Citeseer 1973.
[39] Ju J, Morgan RJ. Characterization of microcrack development in BMI-carbon fiber composite under stress and thermal cycling. J Compos Mater 2004;38(22):2007–24.
[40] Da Silva LFM, Adams RD. Stress-free temperature in a mixed-adhesive joint. J Adhes Sci Technol 2006;20(15):1705–26.
[41] Manson SS. Behavior of materials under conditions of thermal stress; 1954.
[42] Coffin Jr LF. A study of the effects of cyclic thermal stresses on a ductile metal. Trans ASME 1954;76:931–50.
[43] Basquin OH. The exponential law of endurance tests. Proc ASTM 1910:625–30.
[44] Christ H-J. Wechselverformung von metallen: zyklisches spannungs-dehnungs-verhalten und mikrostruktur. Springer-Verlag; 2013.